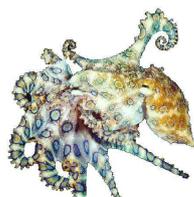# 8   SCIENTIFIC HIGHLIGHT OF THE MONTH: "Octopus: a tool for the application of time-dependent density functional theory"

octopus: a tool for the application of time-dependent density functional theory

Alberto Castro,[a,f] Miguel A. L. Marques[b,f], Heiko Appel[a,f], Micael Oliveira[b,f],
Carlo A. Rozzi[c,f], Xavier Andrade[d,e,f], Florian Lorenzen[a], E. K. U. Gross[a,f] and Angel
Rubio.[e,a,f]

[a] Institut für Theoretische Physik, Fachbereich Physik, Freie Universität Berlin, Deutschland.
[b] Departamento de Física, Universidade de Coimbra, Coimbra, Portugal.
[c] CNR-INFM National Research Center on nanoStructures and bioSystems at Surfaces (S3),
Modena, Italia.
[d] Laboratoire des Solides Irradiés, École Polytechnique, Paris, France
[e] Departamento de Física de Materiales, Facultad de Ciencias Químicas, UPV/EHU, Centro
Mixto CSIC-UPV/EHU and Donostia International Physics Center, E-20018 San Sebastián,
España.
[f] European Theoretical Spectroscopy Facility (ETSF).

Abstract

We report on the background, current status, and current lines of development of the
octopus project. This program materializes the main equations of density-functional theory
in the ground state, and of time-dependent density-functional theory for dynamical effects.
The focus is nowadays placed on the optical (i.e. electronic) linear response properties of
nanostructures and biomolecules, and on the non-linear response to high-intensity fields of
finite systems, with particular attention to the coupled ionic-electronic motion (i.e. photo-
chemical processes). In addition, we are currently extending the code to the treatment of
periodic systems (both to one-dimensional chains, two-dimensional slabs, or fully periodic
solids), magnetic properties (ground state properties and excitations), and to the field of
quantum-mechanical transport or "molecular electronics." In this communication, we con-
centrate on the development of the methodology: we review the essential numerical schemes
used in the code, and report on the most recent implementations, with special attention
to the introduction of adaptive coordinates, to the extension of our real-space technique to
tackle periodic systems, and on large-scale parallelization. More information on the code, as
well as the code itself, can be found at http://www.tddft.org/programs/octopus/.

1 Introduction

Both density-functional theory (DFT) [1,2], and time-dependent density-functional theory (TDDFT) [3, 4] have enjoyed a steady increase of their popularity ever since they were born, in the sixties and eighties respectively. The reason is that both theories achieve, for many problems, an unparalleled balance between accuracy and computational cost. Although the scope of applicability of traditional Quantum Chemistry techniques, or of Quantum Monte-Carlo procedures, have also increased in recent years [5,6], DFT/TDDFT is still the method of choice for large systems (e.g., molecular systems of biological interest) undergoing complex processes.

Correspondingly, numerous software packages that solve DFT/TDDFT equations are available [7]. Among them, `octopus` [8] is one with special focus on TDDFT. In the present newsletter, we describe the current status of this project, and the aims of its developing process. In brief, some of the key aspects that describe `octopus` are:

Target problems:

(i) Linear optical (i.e. electronic) response of molecules or clusters.

(ii) Non-linear response to classical high-intensity electromagnetic fields, taking into account both the ionic and electronic degrees of freedom.

(iii) Ground-state and excited state electronic properties of systems with lower dimensionality, such as quantum dots.

(iv) Photo-induced reactions of molecules (e.g., photo-dissociation, photo-isomerization, etc).

(v) In the immediate future, extension of these procedures to systems that are infinite and periodic in one or more dimensions (polymers, slabs, nanotubes, solids), and to electronic transport.

Theoretical base:

(i) The underlying theories are DFT and TDDFT. Also, the code may perform dynamics by considering the classical (i.e. point-particle) approximation for the nuclei. These dynamics may be non-adiabatic, since the system evolves following the Ehrenfest path. It is, however, a mean-field approach.

(ii) Regarding TDDFT, we have implemented two different approaches: On the one hand, the "standard" TDDFT-based linear-response theory, which provides us with excitation energies and oscillator strengths for ground-state to excited-state transitions. On the other hand, we have also implemented the explicit time-propagation of the TDDFT equations, which allows for the use of large external potentials, well beyond the range of validity of perturbation theory.

Methodology

(i) As numerical representation, we have chosen to work without a basis set, relying on numerical meshes. Nevertheless, auxiliary basis sets (plane waves, atomic orbitals) are used when necessary.

Recently, we have added the possibility of working with non-uniform grids, which adapt to the inhomogeneity of the problem, and of making use of multigrid techniques to accelerate the calculations. The adaptive coordinates implementation will be discussed in some detail in Section 4.

(ii) For most calculations, the code relies on the use of pseudopotentials [9]. We currently allow for two types: Troullier-Martins [10], and Hartwigsen-Goedecker-Hutter [11].

(iii) In addition to being able to treat systems in the standard 3 dimensions, 2D and 1D modes are also available. These are useful for studying, e.g., the two-dimensional electron gas that characterizes a wide class of quantum dots.

Technical aspects

(i) The code has been designed with emphasis on parallel scalability. In consequence, it allows for multiple task divisions. We will comment on this aspect in Section 5.

(ii) The language of most of the code is Fortran 90 (almost 50.000 lines at present). Other languages, such as C or Perl, are also used.

(iii) We have struggled to employ only standard and portable tools. The resulting code may run on virtually any Unix-like platform.

(iv) The package is licensed under the GNU General Public License (GPL). In consequence, it is available for use, inspection, and modification for anyone, at `http://www.tddft.programs/octopus/`.

Section 2 summarizes the algorithms used for ground-state calculations, while the next section handles response properties. Sections 4, 5 and 6 report some of the recent additions to the package: adaptive coordinates to numerically represent the problem, support for parallel calculations (a lot of effort is being put onto the scalability of the computations to large number of processors), and the treatment of periodic systems.

2   Ground-state DFT calculations

2.1   The Kohn-Sham equations

Kohn-Sham (KS) DFT [1, 2] provides the ground state one-particle density n_0 of a system of N electrons exposed to an external potential $v(\vec{r})$, by identifying it with the density of a non-interacting system of electrons subject to the so-called KS potential, $v_{KS}(\vec{r})$. This system, being non-interacting, may be solved through a set of one-particle equations, the KS equations [1] (atomic units will be used throughout):

$$h_{KS}\, \varphi_i(\vec{r}) = \varepsilon_i \varphi_i(\vec{r}) \qquad (i = 1, \ldots, N)\,, \tag{1}$$

$$n_0(\vec{r}) = \sum_{i=1}^{N} |\varphi_i(\vec{r})|^2\,. \tag{2}$$

The functions φ_i and the real numbers ε_i are the KS orbitals and KS eigenvalues, respectively. The KS state is the single Slater determinant built from those orbitals. The KS Hamiltonian is given by

$$h_{\mathrm{KS}}[n] = -\frac{1}{2}\nabla^2 + v_{\mathrm{KS}}(\vec{r})\,. \tag{3}$$

The first term, the kinetic operator, is approximated in a real-space formulation by a *finite difference* formula – details about this will be given in Section 4. The KS potential is usually separated as follows:

$$v_{\mathrm{KS}}(\vec{r}) = v(\vec{r}) + v_{\mathrm{Hartree}}[n](\vec{r}) + v_{\mathrm{xc}}[n](\vec{r})\,. \tag{4}$$

External potential. The external potential $v(\vec{r})$ is typically the sum of the Coulomb potential generated by each of the nuclei. In a pseudopotential formulation, this includes both local and non-local components. For an atom α positioned at $\vec{R}_\alpha$, the pseudopotential $\hat{v}_\alpha(\vec{R}_\alpha)$ is the sum of a local operator $v_\alpha^{\mathrm{local}}$ and a set of non-local projectors described by atom-centered functions ξ_α^κ:

$$\langle \vec{r}|\hat{v}_\alpha(\vec{R}_\alpha)|\varphi\rangle = v_\alpha^{\mathrm{local}}(\vec{r} - \vec{R}_\alpha)\varphi(\vec{r}) + \sum_\kappa \langle \xi_\alpha^\kappa(\vec{R}_\alpha)|\varphi\rangle \xi_\alpha^\kappa(\vec{r} - \vec{R}_\alpha)\,. \tag{5}$$

Note that these projectors are typically well localized in real space, so their action is computationally feasible and faster than in a plane wave formulation.

The code also allows for other "user-defined" external potentials. For example, one can attempt to model the solvent environment of a given system with the electrostatic potential generated by a set of point charges and/or dipoles (e.g. to model a chromophore in its protein environment [12]). This is the basic principle of the so-called QM/MM techniques [13]. Also, the user may define a model potential describing a two-dimensional quantum dot, and can specify it simply by writing down its mathematical function in the input file.

Hartree potential. The second term of (4), $v_{\mathrm{Hartree}}[n](\vec{r})$ is more time-consuming. There are various ways of obtaining this potential numerically, and we have investigated and implemented some of them [14]. These are explained in more detail in Section 2.2.

Exchange-correlation potential. The exchange-correlation (xc) potential, $v_{\mathrm{xc}}[n_0]$, is an unknown functional of the density, and has to be approximated. It is the first functional derivative of the exchange-correlation *energy* functional:

$$v_{\mathrm{xc}}[n](\vec{r}) = \frac{\delta E_{\mathrm{xc}}}{\delta n(\vec{r})}\,. \tag{6}$$

We have incorporated in octopus a wide variety of possible functionals, ranging from the standard local density approximation (LDA) [15] and generalized gradient approximations [16], to the state-of-the-art orbital-dependent functionals [17–19]. "Traditional" LDAs and GGAs are easy, since they are explicit functionals of the density and its gradient. The more recent orbital-dependent functionals, however, are explicit functionals of the KS orbitals (and so they are implicit functionals of the density *through* the orbitals) and require the use of the optimized effective potential method (OEP) [17, 18]. We have implemented these functionals in octopus.

Both the Krieger, Li and Iafrate (KLI) [19] approximation and the full solution of the OEP equation [20] (still in experimental phase) are available.

We are now extending the set of functionals to cope with current-density functionals [21]. At this point, we emphasize that along with the `octopus` distribution we provide a standard "exchange and correlation library," written in C. All (TD)DFT codes require an equivalent piece of software, and in our opinion, it would be mutually beneficial to share an open, reliable library. We expect that this may be a first step towards this goal.

Eigensolvers. Once we know how to construct the real-space representation of the Hamiltonian for a "trial" density n (or, in fact, for a trial set of KS orbitals φ_i from which the density is generated), we are faced with the problem of solving the Kohn-Sham equations (1) for the N lowest lying eigenpairs of this Hamiltonian operator. In real space this amounts to the solution of an eigenproblem for large sparse matrices. The literature in this field is abundant [22], and we have tried several schemes in `octopus`. The following are available in the current version of the code: conjugate-gradients based schemes [23], Lanczos-based algorithms [24] and the Jacobi-Davidson procedure [25].

Mixing. We are left with the mixing of the density, which is essential for the convergence of the self-consistent procedure. For that purpose, we employ some standard techniques. Essentially, one has to build recursively a series of densities $n^{(i)}$ that converges to the solution density n_0. Each new density is generated through a prescription of the form:

$$n^{(i+1)} = G[\tilde{n}^{(i+1)}, n^{(i)}, n^{(i-1)}, \ldots, n^{(i-s)}], \tag{7}$$

where $\tilde{n}^{(i+1)}$ is the density obtained from Eq. (2) using the Kohn-Sham orbitals of step $i+1$. The simplest example of such a prescription is the so-called "linear mixing" [26], for which Eq. (7) takes the form: $n^{(i+1)} = (1-\alpha)\tilde{n}^{(i+1)} + \alpha n^{(i)}$. However, `octopus` allows for more sophisticated procedures – we refer the reader to the original references: the generalized Broyden algorithm of Johnson [27], and the "guaranteed reduction" Pulay algorithm [28].

Spin. All the previous equations were written considering no spin polarization. However, `octopus` is also able to perform calculations using spin-density functional theory, either considering complete spin alignment throughout the system or not. This latter case requires the use of the generalized local spin-density theory [29]. The wave functions are then described as two-component spinors $\Phi(\vec{r}) = (\varphi_1(\vec{r}), \varphi_2(\vec{r}))$ where the components are complex wave functions.

Finally we also mention the possibility to perform calculations including external magnetic fields. As noted above, current-density functionals are being implemented, but it is already possible to perform calculations including a static uniform magnetic field.

2.2 The Hartree potential

In 3 dimensions, the Hartree potential may be represented in two equivalent forms: as the integral:

$$v_{\text{Hartree}}[n](\vec{r}) = \int d^3 r' \frac{n(\vec{r'})}{|\vec{r} - \vec{r'}|}, \tag{8}$$

or as the solution of Poisson's equation:

$$\nabla^2 v_{\text{Hartree}}[n](\vec{r}) = -4\pi n(\vec{r}). \tag{9}$$

There are various ways in which these equations may be solved, and we have investigated and implemented some of them [14].

Conjugate gradients. This amounts to solving Eq. (9) via a conjugate gradients algorithm. This poses the problem of the boundary conditions for v. The standard solution is to obtain the boundary conditions by calculating the value of v at points around the simulation box by making use of a multipole expansion representation of the density n: For points outside, the potential is given by

$$v_{\text{Hartree}}(\vec{r}) = \sum_{l=0}^{\infty} \sum_{m=-l}^{l} \frac{4\pi}{2l+1} \frac{1}{r^{(l+1)}} Y_{lm}(\hat{r}) Q_{lm}, \tag{10}$$

$$Q_{lm} = \int d^3 r\, r^l Y_{lm}(\vec{r}) n(\vec{r}),$$

where Y_{lm} are spherical harmonics. `octopus` now offers an alternative: we subtract from n a sum of densities $Q_{lm} n_{lm}$, where Q_{lm} are the multipoles of n, and where n_{lm} are auxiliary known charge distributions whose (lm)-moment is unity, and whose other moments are zero:

$$\bar{n} = n - \sum_{l=0}^{L} \sum_{m=-l}^{l} Q_{lm} n_{lm}. \tag{11}$$

For a sufficiently large integer L, $\bar{n}$ has negligible boundary conditions, so that $v_{\text{Hartree}}[\bar{n}]$ may be calculated with the usual Laplacian with zero boundary conditions. Since Poisson's equation is linear,

$$v_{\text{Hartree}}[n] = v_{\text{Hartree}}[\bar{n}] + \sum_{l=0}^{L} \sum_{m=-l}^{l} Q_{lm} v_{\text{Hartree}}[n_{lm}]. \tag{12}$$

The functions $v_{\text{Hartree}}[n_{lm}]$ can be obtained exactly (see Ref. [14] for explicit analytical expressions for n_{lm} and $v_{\text{Hartree}}[n_{lm}]$).

Multigrids. Still in real-space, as a recent addition, `octopus` now also allows for the use of the multigrid method [30, 31]. Multigrid is a linear scaling iterative method to solve elliptic problems. The base of this scheme is to use a group of different grids that have less points than the original grid where the problem is discretized. In these coarser grids the corrections to the solution in the original grid are calculated using standard relaxation methods (such as Gauss-Jacobi or Gauss-Seidel). The solution process is much faster in the coarser grids, not only because of the reduced number of points, but also because relaxation operators are less local.

Currently, this technique is implemented in `octopus` only for the problem of solving Poisson's equation; our plans however are to use this technique to accelerate the convergence of our eigensolvers [32, 33].

Fourier space. `octopus` also allows to move to Fourier space and obtain the Hartree potential by making use of the well-known fact that it is simply a multiplicative function in Fourier space. This is be the best choice for fully periodic systems, since it naturally handles the periodic boundary conditions. It is a fast and efficient method thanks to the existence of the Fast Fourier Transform (FFT) algorithm.

For systems of reduced periodicity (finite systems, slabs, cylinders) plane waves can still be used efficiently to calculate the Hartree potential using the cutoff technique. The discussion of this issue is referred to Section 6.

3 Response calculations

3.1 Time-dependent DFT

TDDFT [3,4] extends the previous formulation to time-dependent phenomena; one can establish an analogous mapping between the interacting and a non-interacting system, and we obtain a set of time-dependent one-particle equations [3] (Runge-Gross equations, or time-dependent KS equations, TDKS):

$$i\frac{\partial}{\partial t}\varphi_i(\vec{r}, t) = h_{\mathrm{KS}}(t)\,\varphi_i(\vec{r}) \qquad (i = 1, \ldots, N)\,. \tag{13}$$

$$n(\vec{r}, t) = \sum_{i=1}^{N} |\varphi_i(\vec{r}, t)|^2\,. \tag{14}$$

The KS Hamiltonian is similar to the static version given by Eq. (3):

$$h_{\mathrm{KS}}(t) = -\frac{1}{2}\nabla^2 + v(\vec{r}, t) + v_{\mathrm{Hartree}}[n](\vec{r}, t) + v_{\mathrm{xc}}[n](\vec{r}, t)\,. \tag{15}$$

Note, however, that in this case we allow for an explicitly time-dependent external potential $v(\vec{r}, t)$. The exchange and correlation term is now both a functional of the time-dependent density and of the initial state of the system (typically the ground state). In principle, v_{xc} should depend on the densities at all times in the past; in practice most applications of TDDFT rely on an *adiabatic* approximation:

$$v_{\mathrm{xc}}[n](\vec{r}, t) = v_{\mathrm{xc}}^{\mathrm{gs}}[\rho]\big|_{\rho=n(\vec{r}, t)}\,, \tag{16}$$

where $v_{\mathrm{xc}}^{\mathrm{gs}}$ is the ground state exchange and correlation potential functional. In this way, all the approximations implemented in the code for the ground state calculations translate immediately to the time-dependent formalism. Moreover, orbital functionals are also implemented in `octopus` for time-dependent calculations within the time-dependent KLI scheme [34].

Most applications of TDDFT are restricted to a linearized form of Eqs. (13) and (14) that assumes a small external perturbation, and attempts to obtain the first-order density-density

response in frequency domain. In `octopus` we allow for both possibilities: the linear-response formalism, and the explicit integration of the TDKS equations in the time domain. The latter may not only be used to calculate linear response properties, but also permits to use high-intensity fields and to perform combined electron-ion dynamical simulations.

For the explicit integration of Eqn. (13) in real time one uses a propagation algorithm. In other words, we seek a numerical representation of the evolution operator $\hat{U}(t + \Delta t, t)$:

$$\varphi(\vec{r}, t + \Delta t) = \hat{U}(t + \Delta t, t)\varphi(\vec{r}, t). \tag{17}$$

In TDDFT we are dealing with the integration of a set of coupled Schrödinger-like equations, characterized by two important facts: (i) The Hamiltonian is intrinsically time-dependent, even if there is no external potential, since the Hartree and xc parts depend on the time-dependent density; (ii) The Hamiltonian – at least a part of it – is not known *a priori*: both Hartree and xc terms depend on the solution itself.

For time-independent Hamiltonians, it is well known that the problem reduces to the calculation of the action of the exponential of the Hamiltonian on the function that describes the state. Unfortunately, since this is not the case in TDDFT, one has to approximate the full evolution operator:

$$\hat{U}(t + \Delta t, t) = \sum_{n=0}^{\infty} \frac{(-\mathrm{i})^n}{n!} \int_t^{t+\Delta t} \mathrm{d}t_1 \dots \int_t^{t+\Delta t} \mathrm{d}t_n \mathcal{T}[\hat{h}_{\mathrm{KS}}(t_1) \dots \hat{h}_{\mathrm{KS}}(t_n)], \tag{18}$$

where $\mathcal{T}$ is the time-ordering product. We have done some research on this topic, by implementing in the `octopus` package a handful of algorithms: polynomial expansions (in the standard base or in the Chebyshev base) to approximate the exponential operator, Krylov subspace projections, the split-operator technique, higher-order split-operator-like schemes, the implicit midpoint rule, the exponential midpoint rule, and the so-called Magnus expansions.

For more details on these propagation algorithms, we refer the reader to our publication on the issue [35].

3.2 Electronic excitations by means of time-propagation

Dynamical polarizability. In `octopus` the calculation of the dynamical polarizability can be performed by propagating in real time [36]. This methodology scales well with the size of the system, and is thus our preferred scheme for large systems. Let us recall the essentials of this formulation. We will restrict hereafter to electrical (spin-independent) dipole perturbations:

$$\delta v_{\mathrm{ext},\sigma}(\vec{r}, \omega) = -x_j \kappa(\omega). \tag{19}$$

This defines an electrical perturbation polarized in the direction j: $\delta\vec{E}(\omega) = \kappa(\omega)\hat{e}_j$. The response of the system dipole moment in the i direction

$$\delta\langle\hat{X}_i\rangle(\omega) = \sum_{\sigma} \int \mathrm{d}^3 r \, x_i \, \delta n_{\sigma}(\vec{r}, \omega) \tag{20}$$

is then given by:

$$\delta\langle\hat{X}_i\rangle(\omega) = -\kappa(\omega) \sum_{\sigma\sigma'} \int \mathrm{d}^3 r \int \mathrm{d}^3 r' \, x_i \, \chi_{\sigma\sigma'}(\vec{r}, \vec{r}', \omega) \, x_j'. \tag{21}$$

We may define the dynamical dipole polarizability $\alpha_{ij}(\omega)$ as the quotient of the induced dipole moment in the direction i with the applied external electrical field in the direction j, which yields:

$$\alpha_{ij}(\omega) = -\sum_{\sigma\sigma'}\int d^3r \int d^3r'\, x_i\, \chi_{\sigma\sigma'}(\vec{r}, \vec{r}', \omega)\, x_j' \,. \tag{22}$$

The dynamical polarizability elements may then be arranged to form a second-rank symmetric tensor, $\boldsymbol{\alpha}(\omega)$. The cross-section tensor is proportional to its imaginary part:

$$\boldsymbol{\sigma}(\omega) = \frac{4\pi\omega}{c}\Im\boldsymbol{\alpha}(\omega) \,. \tag{23}$$

We consider a sudden external perturbation at $t = 0$ (delta function in time), which means $\kappa(\omega) = \kappa$, equal for all frequencies. This perturbation is applied along a given polarization direction, say $\hat{e}_j$. By propagating the time-dependent Kohn-Sham equations, we obtain $\delta\langle\hat{X}_i\rangle(\omega)$ through Eq. (20). The polarizability element $\alpha_{ij}(\omega)$ may then be calculated easily via:

$$\alpha_{ij}(\omega) = -\frac{\delta\langle\hat{X}_i\rangle(\omega)}{\kappa} = -\frac{1}{\kappa}\int d^3r\, x_i\, \delta n(\vec{r}, \omega). \tag{24}$$

Symmetry considerations. One recent addition to `octopus` [37] is the possibility of taking advantage of the possible symmetries of a given molecule when calculating its dynamical polarizability tensor, Eq. (22), through the time-propagation technique.

Let us consider three linearly-independent, but possibly not non-orthogonal, unit vectors $\{\hat{p}_1, \hat{p}_2, \hat{p}_3\}$. We define the polarizability elements $\tilde{\alpha}_{ij}(\omega)$ as:

$$\tilde{\alpha}_{ij}(\omega) = -\int d^3r \int d^3r'\, (\vec{r}\cdot\hat{p}_i)\chi(\vec{r}, \vec{r}', \omega)(\vec{r}'\cdot\hat{p}_j) \,. \tag{25}$$

This corresponds to a process in which the polarization of the perturbing field is along $\hat{p}_j$, and the dipole is measured along $\hat{p}_i$. If we know the 3x3 matrix $\tilde{\boldsymbol{\alpha}}(\omega)$, we can get the *real* tensor $\boldsymbol{\alpha}(\omega)$ by making use of the following simple relationship, which can be obtained once again from Eq. (22):

$$\tilde{\boldsymbol{\alpha}}(\omega) = \mathbf{P}^t\boldsymbol{\alpha}(\omega)\mathbf{P} \,. \tag{26}$$

$\mathbf{P}$ is the transformation matrix between the original orthonormal reference frame and $\{\hat{p}_1, \hat{p}_2, \hat{p}_3\}$. Note, that this transformation is in general not a rotation, as $\mathbf{P}$ is not unitary. Moreover, no matter how familiar it looks, Eq. (26) does not describe a change of coordinates: $\tilde{\boldsymbol{\alpha}}(\omega)$ is *not* the polarizability tensor in the new reference frame. And finally, also note that the traces of $\tilde{\boldsymbol{\alpha}}$ and $\boldsymbol{\alpha}$ do not coincide:

$$\text{Tr}\left[\tilde{\boldsymbol{\alpha}}(\omega)\right] = \text{Tr}\left[\mathbf{P}^t\boldsymbol{\alpha}(\omega)\mathbf{P}\right] = \text{Tr}\left[\boldsymbol{\alpha}(\omega)\mathbf{P}\mathbf{P}^t\right] \,. \tag{27}$$

but $\mathbf{P}\mathbf{P}^t \neq \mathbf{1}$. Notwithstanding all this, it is the basis of our scheme, since it tells us that we may obtain the polarizability tensor by obtaining the related object $\tilde{\boldsymbol{\alpha}}(\omega)$.

Now let us assume that the molecule under study possesses some non-trivial symmetry transformations – to start with, we consider that it has two, $\mathcal{A}$ and $\mathcal{B}$. We consider an initial unit vector, $\hat{p}_1$, and define:

$$\hat{p}_2 = \mathcal{A}\hat{p}_1 \tag{28}$$
$$\hat{p}_3 = \mathcal{B}\hat{p}_2$$

153

We assume that this may be done in such a way that the set $\{\hat{p}_1, \hat{p}_2, \hat{p}_3\}$ is linearly independent. Next, we perform a TDDFT calculation with the perturbing field polarized in the direction $\hat{p}_1$. This permits us to obtain the row $\{\tilde{\alpha}_{11}, \tilde{\alpha}_{12}, \tilde{\alpha}_{13}\}$. Since the matrix is symmetric, we also have the column $\{\tilde{\alpha}_{11}, \tilde{\alpha}_{21}, \tilde{\alpha}_{31}\}$. The symmetry of the molecule also permits us to obtain the diagonal: $\{\tilde{\alpha}_{33} = \tilde{\alpha}_{22} = \tilde{\alpha}_{11}\}$. The only missing element is $\tilde{\alpha}_{23} = \tilde{\alpha}_{32}$, but it is easy to prove that:

$$\tilde{\alpha}_{23} = \det(\mathcal{A}) \ \tilde{\alpha}_{1, \mathcal{A}^{-1}\hat{p}_3}, \tag{29}$$

which we can also obtain from our original calculation. The conclusion is that we have access to the full tensor by performing only one calculation.

Finally, we should note that these symmetry considerations may be extended to other response properties of the system, and to the calculation of the singlet and triplet excitations of paramagnetic molecules.

3.3   Electronic excitations by means of linear-response theory

We recall here the fundamental equations of the linear response formalism [38]. In the following, we work directly in the frequency domain – the variable ω denotes the frequency. A small perturbation $\delta v_\sigma(\vec{r}, \omega)$ will induce a density response $\delta n_\sigma(\vec{r}, \omega)$ (hereafter the Greek letters σ, τ, μ will denote spin components). They will be linearly related by the susceptibility function:

$$\delta n_\sigma(\vec{r}, \omega) = \sum_{\sigma'} \int \mathrm{d}^3 r' \chi_{\sigma\sigma'}(\vec{r}, \vec{r}', \omega) \delta v_{\sigma'}(\vec{r}', \omega). \tag{30}$$

An analogous equation may be written for the KS system, substituting the interacting susceptibility by the KS susceptibility $\chi_{\sigma\sigma'}^{\mathrm{KS}}$ and the external perturbation δv_σ by the KS variation $\delta v_{\mathrm{KS},\sigma}$. The density response, however, is identical by virtue of the Runge-Gross theorem [3]. The KS variation is:

$$\delta v_{\mathrm{KS},\sigma}(\vec{r}) = \delta v(\vec{r}) + \int \mathrm{d}^3 r' \frac{\delta n(\vec{r}')}{|\vec{r} - \vec{r}'|} + \sum_{\sigma'} \int \mathrm{d}^3 r' f_{\mathrm{xc},\sigma\sigma'}(\vec{r}, \vec{r}', \omega) \delta n_{\sigma'}(\vec{r}', \omega), \tag{31}$$

where the so-called "kernel", $f_{\mathrm{xc},\sigma\sigma'}(\vec{r}, \vec{r}', \omega)$, is the second functional derivative of the xc energy functional. If we now make use of the identity between densities of the real and of the KS systems, we arrive at a Dyson-like equation for the response function [39]:

$$\chi_{\sigma\sigma'}(\vec{r}, \vec{r}', \omega) = \chi_{\sigma\sigma'}^{\mathrm{KS}}(\vec{r}, \vec{r}', \omega) + \sum_{\tau\tau'} \int \mathrm{d}^3 r \int \mathrm{d}^3 r' \chi_{\sigma\tau}(\vec{r}, \vec{x}, \omega) \left[\frac{1}{|\vec{x} - \vec{x}'|} + f_{\mathrm{xc},\tau\tau'}(\vec{x}, \vec{x}', \omega) \right] \chi_{\tau'\sigma'}^{\mathrm{KS}}(\vec{x}', \vec{r}', \omega). \tag{32}$$

A fully self-consistent solution of this equation would provide us with the response function of the interacting system. Unfortunately, this is quite difficult numerically. Furthermore, it requires the knowledge of the non-interacting response function, $\chi_{\sigma\sigma'}^{\mathrm{KS}}$. This function is usually evaluated through an infinite summation over both occupied and unoccupied KS states. This summation may be slowly convergent. For systems with a discrete spectrum of excitations (like finite systems), it is possible to recast this equation through a series of transformations [38] into a form that is manageable and resembles the equations that are obtained in the time-dependent

Hartree-Fock and Bethe-Salpeter approaches in many-body perturbation theory [42]. We write here only the final result – which is the equation that `octopus` actually solves:

$$\mathbf{\Omega}\vec{F}_I = \Omega_I^2\vec{F}_I \,. \tag{33}$$

This is an eigenvalue equation of dimension N_{pairs}, where N_{pairs} is the number of pairs of occupied and unoccupied KS orbitals that one wishes to consider (ideally infinite). The matrix $\mathbf{\Omega}$ is defined as:

$$\Omega_{ia\sigma,jb\mu} = \delta_{ij}\delta_{ab}\delta_{\sigma\mu}(\varepsilon_{a\sigma} - \varepsilon_{i\sigma})^2 + 2\sqrt{\varepsilon_{a\sigma} - \varepsilon_{i\sigma}}K_{ia\sigma,jb\mu}\sqrt{\varepsilon_{b\sigma} - \varepsilon_{j\mu}}\,, \tag{34}$$

with the matrix elements

$$K_{ia\sigma,jb\mu} = \int \mathrm{d}^3 r \int \mathrm{d}^3 r' \, \varphi_{i\sigma}^*(\vec{r})\varphi_{a\sigma}(\vec{r}) \left[\frac{1}{|\vec{r} - \vec{r}'|} + f_{\text{xc},\sigma\mu}(\vec{r},\vec{r}')\right] \varphi_{j\mu}^*(\vec{r})\varphi_{b\mu}(\vec{r})\,. \tag{35}$$

Here i and j run over occupied KS states, a and b over unoccupied KS states, and σ and μ are spin indexes. Upon diagonalization of this matrix, we obtain the eigenvalues Ω_I^2, which are the squares of the excitation energies of the system. The eigenvectors, in turn, contain the information that permits to obtain the transition densities and the oscillator strengths of these excitations.

We should remark, however, that Eq. (33) assumes that the $\mathbf{\Omega}$ matrix is independent of the excitation energy. This is an approximation: For exchange-correlation potentials with memory (e.g. Ref. [40]), one has to solve self-consistently a non-linear eigenvalue problem: $\mathbf{\Omega}(\Omega_I)\vec{F}_I = \Omega_I^2\vec{F}_I$, whose manifold of solutions is usually larger than the approximated one.

In order to implement the TDDFT-based linear-response equations – essentially, Eq. (33) –, one just needs to provide a means to calculate the $\mathbf{\Omega}$ matrix elements in Eq. (34). The only new difficulty is the appearance of a new ingredient, the kernel $f_{\text{xc}}(\vec{r},\vec{r}')$. Note that this is a two-point function, although it reduces to a one-point function in local approximations to the exchange and correlation energy functionals.

3.4 High-intensity fields

Now, a word about calculations in the non-linear regime (i.e. when applying large external electromagnetic fields, or when studying the scattering of a high energy projectile by a molecule). One external field is added to the "internal" KS potential; In such cases the external potential takes typically the form:

$$v(\vec{r},t) = E_0 f(t)\sin(\omega t)\hat{\mathbf{p}} \cdot \vec{r}. \tag{36}$$

This ansatz describes a classical laser pulse in the dipole approximation, where f is the "envelope" of the pulse and $\hat{\mathbf{p}}$ is the polarization of the light. Finally, E_0 determines the intensity of the pulse. Of course there is no problem to extend this ansatz in order to describe more general situations.

When dealing with high-intensity fields, there will be a non-negligible transition probability to unbound states. In other words, the incoming field may induce the ionization of part of the electronic cloud. The observables related to this process are the ionization probabilities, which are functionals of the time-dependent density by virtue of the Runge-Gross theorem.

Unfortunately, these functionals are unknown. There is not a fully satisfactory way to deal with this issue within a grid-based formalism, but there are some approximate methods that rely on a geometrical picture [41]: we define a bound region $\mathcal{A}$ around the system that contains the bound states, and the density that travels outside (to the rest of the space, $\mathcal{B}$) corresponds to ionized states.

In practice, there are two schemes to simulate this ionization in `octopus`. The first consists of adding an imaginary potential to the Hamiltonian, which is defined to be non-zero only in a frontier region $\mathcal{F}$ that separates $\mathcal{A}$ and $\mathcal{B}$. It varies smoothly from zero in the intersection of $\mathcal{F}$ and $\mathcal{A}$ to a maximum in the limit of the simulation region. The role of this imaginary potential is to eliminate in a smooth way the electronic density that approaches the frontier of the simulation region. The second uses a mask function to selectively remove the density close to the borders.

A classical example for the application of TDDFT within the high-intensity field regime is the calculation of the High-Harmonic Generation (HHG) spectrum of a molecule: If we shine a very intense laser field (of intensity over $10^{13}\mathrm{W/cm^2}$) on a molecule, an electron may absorb several photons, be ejected, and then return emitting one single photon. This photon has a frequency which is an integer multiple of the frequency of the external driving field. The spectrum of emitted radiation is approximately (i.e. neglecting incoherent processes) given by:

$$\sigma_{\mathrm{emission}}(\omega) = \left| \int \mathrm{d}t e^{-\mathrm{i}\omega t} \frac{\mathrm{d}^2}{\mathrm{d}t^2} \langle \hat{\vec{R}} \rangle \right|^2 . \tag{37}$$

Since the dipole $\langle \hat{\vec{R}} \rangle$ is an explicit functional of the time dependent density, the emission spectrum can then be approximated with TDDFT. A couple of examples may be found in Ref. [43].

3.5   Coupled ion-electron response

In order to study the dynamics of molecules exposed to external fields, we have implemented a mixed classical/quantum approach. The Hellman-Feynman theorem is no longer valid in this case, but we may resort to the Ehrenfest theorem; the model may be described as two coupled dynamical systems: one quantum system of non-interacting particles (the KS/TDDFT system of electrons) subject to the KS potential, and one classical system of particles describing the ions. The first system obeys Eqs. (13) and (14); the second system is described by Newton's equations:

$$m_\alpha \frac{d\vec{R}_\alpha}{dt} = \vec{P}_\alpha , \tag{38}$$

$$\frac{d\vec{P}_\alpha}{dt} = -\sum_j \langle \varphi_j(t) | \vec{\nabla}_{\vec{R}_\alpha} v_{\mathrm{KS}}[n] | \varphi_j(t) \rangle + \sum_{\beta \neq \alpha} \vec{F}_{\beta \to \alpha} . \tag{39}$$

In these equations, m_α is the mass of the nucleus tagged by α; $\vec{R}_\alpha$ and $\vec{P}_\alpha$ are their position and momentum; $\vec{F}_{\beta \to \alpha}$ is the classical electrostatic force exerted by nucleus β on nucleus α. Eq. (39) is nothing else than a reformulation of Ehrenfest's theorem.

3.6 Sternheimer's equations

One recent addition to `octopus` is the possibility of calculating response properties using density-functional perturbation theory [44–46]. Currently it is possible to calculate static polarizabilities and the first hyperpolarizabilities,

The base of this theory is that, for a given perturbative potential, we can find the first order perturbations to the wavefunctions ($\varphi_i^{(1)}$) solving the Sternheimer [47] equation

$$\left(H^{(0)} - \varepsilon^{(0)} \right) \varphi_i^{(1)} = - \left(H^{(1)} - \varepsilon^{(1)} \right) \varphi_i^{(0)} , \tag{40}$$

the $H^{(1)}$ term includes the perturbative potential and the variation of the Hamiltonian due to the variation of the density, which is

$$n^{(1)} \left(\vec{r} \right) = \sum_{i=0}^{N} \left[\varphi_i^{*(0)} \left(\vec{r} \right) \varphi_i^{(1)} \left(\vec{r} \right) + \varphi_i^{*(1)} \left(\vec{r} \right) \varphi_i^{(0)} \left(\vec{r} \right) \right] . \tag{41}$$

The two equations (40) and (41) form a system that must be solved self-consistently. As the right hand side of (40) is known, this is a linear equation that can be solved by iterative methods.

Thanks to the $2n + 1$ theorem [48], using the first order perturbations of the wavefunctions, we are able to calculate properties that are second and third-order derivatives of the total energy (polarizability and the first hyperpolarizability, for instance).

This formalism is also applicable to time dependent perturbations, using TDDFT [49], where we have to solve a slightly different Sternheimer equation

$$\left(H^{(0)} - \varepsilon^{(0)} \pm \omega \right) |\varphi_i^{(1)}\rangle = -H^{(1)}|\varphi_i^{(0)}\rangle , \tag{42}$$

where ω is the frequency of the perturbative potential. We are now developing this scheme to calculate dynamical polarizabilities.

4 Adaptive coordinates

The real-space techniques for computational simulations in the condensed matter realm are usually praised for, at least, two strong advantages: On the first hand, the intrinsically local character of the "basis set" permits, in principle, large scale parallelization by dividing the space in domains. This locality is also the basis for the use of techniques aiming at the linear-scaling of the computational effort. On the second hand, the real space mesh on which the magnitudes are represented may be locally adapted to the needs of each region – one feature which is difficult to translate to the more traditional plane wave representation.

This section is centered on the second aspect: One possible route to implement curvilinear coordinates, able to adapt the local resolution to the needs of each region in space. The next section will be dedicated to the parallelization.

A real-space representation is the description of the functions involved in the calculation by the values that these functions take on a collection of points in real space (the "grid" or "mesh"). This grid can be regular – meaning that the points are equispaced between each other – or
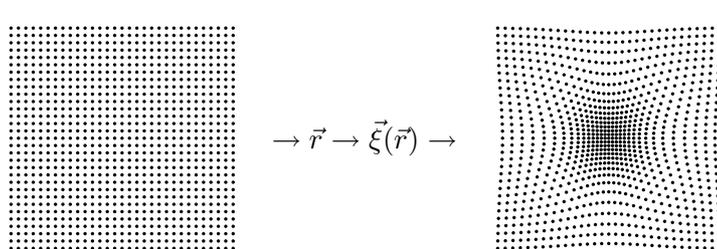
$$\rightarrow \vec{r} \rightarrow \vec{\xi}(\vec{r}) \rightarrow$$

Figure 1: An adaptive-coordinates representation is constructed through the definition of a coordinate transformation function $\vec{\xi}$.
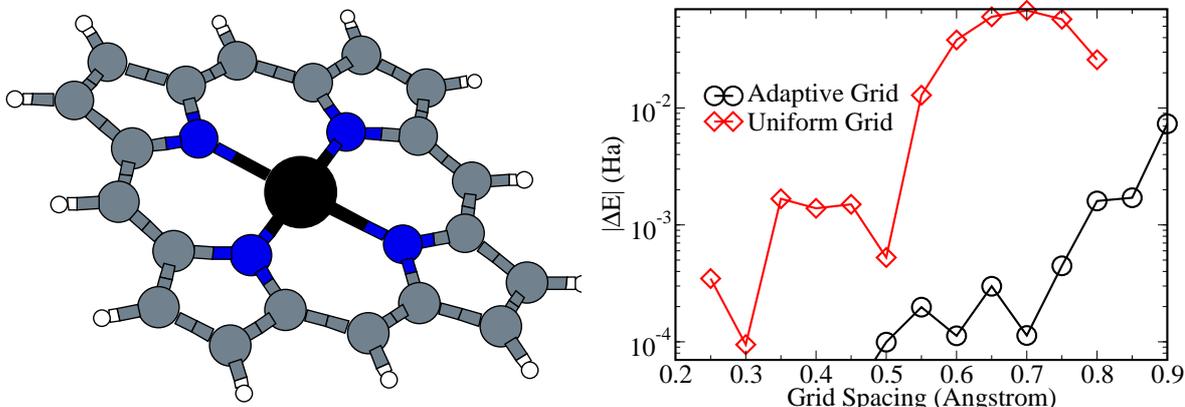

Figure 2: Left: the "basic" porphyrin molecule. Right: convergence study of the ground-state total energy of the porphyrin molecule, with and without the use of the adaptive-grid technique. In this case, we have used the transformation formula of F. Gygi [50], doubling the local cut-off near the atoms, and a 44-point stencil to represent the Laplacian operator.

curvilinear. An "adaptive" or "curvilinear" grid is the deformation of a regular grid through some transformation function (see Fig. 1), which leads to a curved distribution of points. This deformation should be intelligently done, so that the density of points increases in the regions of space where the problem requires a larger resolution.

In the last years, a number of groups have contributed to the development of these techniques in the field of electronic structure calculations. We have specially looked at the works of F. Gygi and collaborators [50], Hamann [51], Pérez-Jordá [52], Briggs and collaborators [53], E. Fattal and collaborators [54] and at the work of Waghmare and collaborators [55]. In octopus we have implemented one scheme based on the ideas of these works.

An example of curvilinear coordinates is based on the following transformation function, first proposed by Gygi [50]

$$\xi^i = x^i + \sum_\alpha (x^i - R_\alpha^i) f_\alpha(|\vec{x} - \vec{R}_\alpha|), \tag{43}$$

$$f_\alpha(r) = A_\alpha \frac{a_\alpha}{r} \tanh\left(\frac{r}{a_\alpha}\right) \exp\left[-\left(\frac{r}{b_\alpha}\right)^2\right], \tag{44}$$

where α runs over the atoms, and $\vec{R}_\alpha$ are the atomic positions. The parameters A_α, a_α, and b_α fine-tune the transformation – what will be the resolution enhancement, the region around each atom where the regular grid is transformed, etc.

Once that the positions of the grid points are specified, we represent each function involved in the calculation $(f, g, \dots)$ by the vector formed by the values that it takes on the grid points

158

$(\mathbf{f}, \mathbf{g}, \ldots)$. We must then define the basic operations:

- The basic vector space operations are of course unaltered: $\alpha f + \beta g \rightarrow \alpha \mathbf{f} + \beta \mathbf{g}$.

- The integration is now a weighted sum; each grid point i has a weight ω_i, which is in fact the Jacobian of the transformations:

$$\int \mathrm{d}^3 r \, f(\vec{r}) = \sum_i \omega_i f_i \,, \tag{45}$$

$$w_i = \det \left[\frac{\partial x_m^i}{\partial r_n} \right] . \tag{46}$$

- The integral permits to define the dot product:

$$\langle f | g \rangle = \sum_i \omega_i f_i g_i = \mathbf{f}^\dagger \mathbf{\Omega} \mathbf{g} \,. \tag{47}$$

We see how a metric appears naturally; it is given by the diagonal matrix $\mathbf{\Omega}$: $\Omega_{ij} = \delta_{ij} \omega_i$.

- The operators that are local in real space are trivial to represent; they are just multiplicative operators in the same way that they were for uniform grids.

- The differential operators (e.g. the kinetic operator) are the main problem. In principle, one can use the transformation laws to relate the differential operators in the new grid to the usual well-known finite-differences discretization expressions in the uniform space:

$$\nabla^2 = \sum_{ij} g^{ij} \frac{\partial}{\partial \xi^i} \frac{\partial}{\partial \xi^j} + \sum_{lik} \frac{\partial \xi^l}{\partial x^k} \frac{\partial}{\partial \xi^l} \left(\frac{\partial \xi^i}{\partial x^k} \right) . \tag{48}$$

This, however, involves a lot of computations, and in general does not provide a Hermitian operator.

Instead, we have used the following approach, valid for any grid, even unstructured ones:

– Select a stencil: given each point in the grid, the stencil is the set of neighboring points from which we calculate the action of any differential operator $\mathcal{D}$:

$$(\mathcal{D}(f))_i = \sum_{j \in \mathrm{Stencil}(i)} C_j^i f_j \,. \tag{49}$$

– Select a set of polynomials $\{x^\alpha y^\beta z^\delta\}$, of equal number to the points in the stencil: the coefficients C_j^i are fixed by ensuring that the action of $\mathcal{D}$ on these polynomials is *exact*.

This amounts to solving a linear system of equations of order the size of the stencil for each point of the grid. This operation must be performed at the beginning of the calculations, or every time that the grid is redefined.

– The Laplacian operator is Hermitian; the gradient operator is anti-Hermitian. The resulting numerical operator $\mathbf{C}$, however, is *not* (anti) Hermitian. But it can be (anti) symmetrized by transforming the matrix $\mathbf{C}$ in the following way:

$$\tilde{\mathbf{C}} = \frac{1}{2} (\mathbf{C} \pm \mathbf{W}^{-1} \mathbf{C} \mathbf{W}) \,. \tag{50}$$
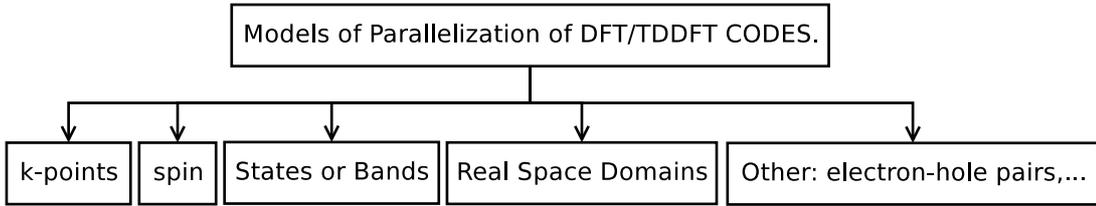
Figure 3: Parallelization modes for DFT/TDDFT codes.

More details about the selection of the stencil and of the fitting polynomials may be consulted directly in the code, and will be provided in a separate publication. Here we will finish this section by presenting an example that shows the gain that is to be expected from the use of adaptive coordinates.

For that purpose we have chosen the "base" porphyrin molecule, depicted on the left hand side of Fig. 2. We have then calculated its ground state total energy at the KS/LDA level, with varying grid spacing. We plot, on the right hand side of Fig. 2, the resulting convergence study – a plot of the error in the total energy as a function of the grid spacing.

We show two curves, one of them corresponds to the calculations with the standard uniform grid, and one of them with adaptive coordinates. The meaning of the grid spacing in the latter case is ambiguous (the spacing is no longer constant), and therefore we plot in the figure the original grid spacing, *before* the transformation is performed. In this way, at each abscissa point the number of grid points of both the uniform and the adaptive grid is the same.

In this case, we used Gygi's transformation function, Eq. (43). The parameters are chosen in such a way that the grid resolution is doubled in the vicinity of the nuclei. The plot shows a faster convergence for the adaptive grid: The calculation can be done, with the same level of accuracy, by making use of roughly half the number of points (it is the number of points in the grid that determines the final computational cost).

5 Large-scale parallelization

The current trend in hardware technology follows a steep increase in the number of processors in each computing machine or facility, as opposed to the trend towards an increase in the clock speed or number of operations that each processing unit may perform per unit time. To use modern computing facilities efficiently, we have to ensure that our codes are able to benefit from such parallel-computing architectures.

5.1 Parallelization strategies

Recently, we have incorporated into `octopus` a multiple-way parallelization scheme that may divide the work among a given number of processors, splitting the tasks either in **k**-points, in Kohn-Sham states, in regions of real-space, or in a combination of all of them. Each single form of the contemplated parallelizations may scale by its very nature only to a certain maximum number of processors. Only combined schemes allow to overcome such limitations.

In Fig. 3 we have represented the various possible modes for which a task division within a DFT/TDDFT calculation may be obtained:

- **k**-points: In a ground-state DFT calculation each processor solves the KS equation

$$\hat{H}_{\mathbf{k}}^{\text{KS}} \, \varphi_{n\mathbf{k}}(\vec{r}) = \varepsilon_{n\mathbf{k}}\varphi_{n\mathbf{k}}(\vec{r}) \tag{51}$$

  for a given but fixed **k**-point. Communication among the nodes is only required for the calculation of the (common) density or other Brillouin-zone integrations. This is the parallelization mode that most ground-state solid-state DFT codes offer. The implementation is straightforward and scales very nicely with the number of processors. However, limitations arise for systems with very large unit cells.

- spin: The different spin subspaces may be treated by different processors. In practice this is rather similar to the **k**-point parallelization, so that both spin and **k**-points are represented as common quantum numbers and are treated on the same footing.

- Kohn-Sham states: For the ground-state a parallelization in state indices or bands is more involved than the **k**-point parallelization. Essentially, the state indices have to be divided into different state-groups. The eigenproblem is then solved for each group and a subsequent orthonormalization of the states is performed among the states of different groups. Special block-diagonalization algorithms are used for this task.

  On the other hand, in time-dependent DFT the parallelization in state indices is straightforward. Since the time-dependent Kohn-Sham equations constitute a N-fold initial value problem, each orbital/state index may be propagated on a different processor. Communication is only required for the calculation of the density and in some cases for the calculation of the current.

- real-space regions: The real-space mesh is divided into different domains, so that each processor can treat a different portion of the total mesh. This is illustrated in the left of Fig. 4, where we show a six-fold domain decomposition of a benzene molecule in the x-y plane. Apart from the distribution of the computational burden over the different nodes, this parallelization strategy also has the distinct advantage that the total memory requirement for the storage of the grid points is distributed over the nodes. Much larger systems can be treated if domain parallelization is used.

  The price one has to pay for this flexibility is the rather involved implementation which requires non-trivial communication among the nodes. On the right hand side of Fig. 4 we show the application of a finite-difference stencil of the Laplacian to a boundary point of Domain B. Due to the non-local character of the stencil this requires points of Domain A (grey shaded area) which are held in memory by a neighboring processor. These points are termed ghost points and need to be communicated among neighboring nodes every time the function values on the grid change. Low-latency high-bandwidth networks are therefore the preferred interconnects for such an implementation.

- other: electron-hole pairs, scattering states, etc: The basis set in a linear response calculation within time-dependent DFT consists of electron-hole pairs: products of occupied and
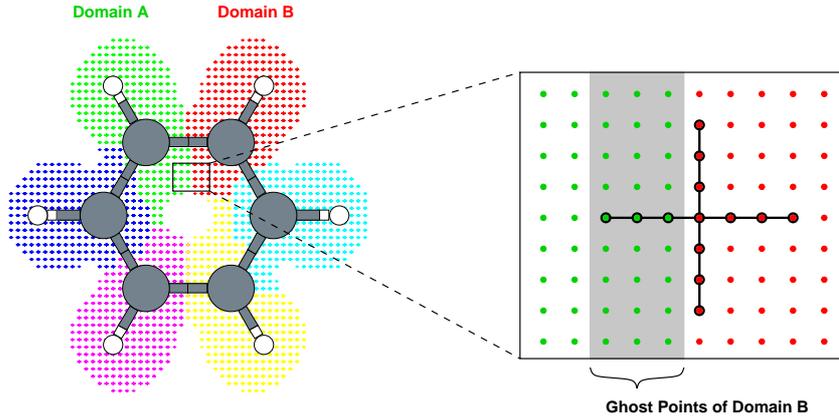
161

Figure 4: Ghost points in a domain parallelization.

unoccupied Kohn-Sham states. Typically a large number of matrix elements in the form of Eq. (34) is required. Since the different matrix elements are independent of each other, a parallelization may be easily obtained by simply distributing their calculation over the different nodes.

The natural description of a quantum-mechanical transport calculation is in terms of scattering states at given energies. Similar in spirit to the parallel treatment of Kohn-Sham states, the propagation of these scattering states can be distributed over different nodes.

5.2 Technical aspects

For the implementation of the multiple-way parallelization in `octopus` we have employed version 1 of the message passing standard MPI [56]. The choice was mainly motivated by the availability of this MPI variant for virtually any computer architecture, and by the fact that MPI is the de facto standard on large-scale parallel architectures. We did not make use of version 2 or newer developments in the MPI standard since these features are still not available on many platforms. Parallelization techniques like OpenMP have been ruled out from the start, since they are limited to shared memory architectures with many processors in a single machine. The current Top500 list [57] contains only a few machines of this kind.

Within `octopus` we allow for various different box shapes like spheres, cylinders or parallelepipeds in 3D, or disks and rectangles in 2D. With a recent addition to the code even arbitrary user-defined shapes can be chosen. To treat the segmentation of the real space mesh for all possible geometries and spatial dimensions on the same footing, we convert the sequence of mesh points into a structured graph. The problem of decomposing the real-space mesh into different domains is then translated into a graph-partitioning problem. Several graph algorithms are available for such tasks and we have chosen for our implementation in `octopus` a "multilevel k-way partitioning algorithm" as provided by the `METIS` library [58]. The library functions try to minimize the edge cuts while the graph partitioning is performed. Translated back to the
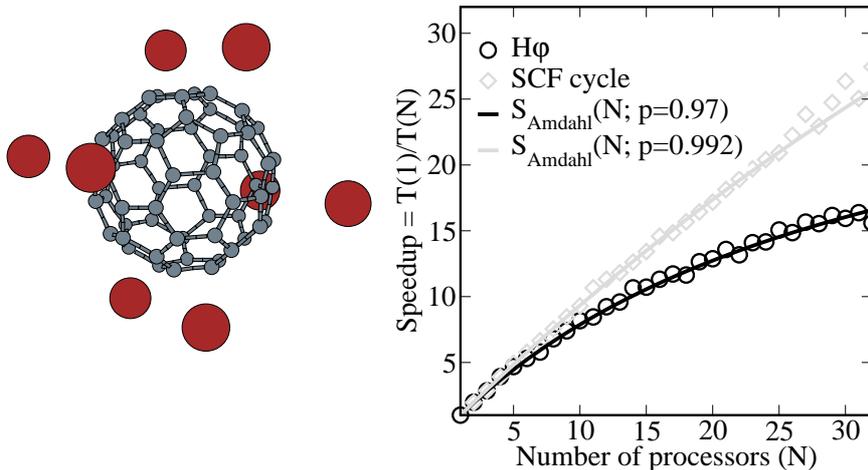
Figure 5: Measured speedups for a domain-parallel calculation of $Cs_8@C_{60}$.

real-space mesh this means that the intersection area of neighboring domains is minimized which in turn implies that fewer ghost points have to be communicated between the different nodes. This effect can be seen nicely in the example of the benzene molecule (Fig. 4) where the domain boundaries computed by `METIS` always lie between two carbon atoms, the optimal situation in this case.

5.3 Application to $Cs_8@C_{60}$

In Fig. 5 we show a sample calculation for 8 Cs atoms attached to C_{60}. Because of the size of the Cs atoms a rather large sphere with 26 Å diameter was used as enclosing computational domain. By choosing a grid spacing of $\Delta=0.20$Å a total number of 1.177.863 grid points were contained in the calculation box.

To asses the performance of the domain parallelization we have repeated the ground-state DFT calculation of this system with a varying number of processors ranging from one to 32. On the right hand side of Fig. 5 we plot the measured speedup as function of the number of processors. The circles correspond to the timings obtained for the application of the Hamiltonian to the wavefunction and the diamonds represent the measured timings for a full SCF cycle. Both curves follow Amdahl's law [59]: Suppose that p is the fraction of a calculation that can be performed in parallel. Then $1 - p$ is the percentage which is intrinsically serial. If we define the speedup $S(N,p)$ of a parallel calculation as the ratio $T(1,p)/T(N,p)$, where $T(N,p)$ is the execution time using N processors, we find

$$S(N,p) = \frac{1}{1 - p + p/N}.$$

(52)

Note, that the speedup will always saturate to $1/(1-p)$ as function of the number of processors, if $p < 1$. In Fig. 5 we have fitted our measured data to Amdahl's law (solid lines) and obtain parallel fractions $p = 0.97$ for the application of $\hat{H}$ to the wavefunction and $p = 0.992$ for the execution of a full SCF cycle. Both fractions indicate that a high degree of parallelization has been achieved for the domain parallelization in `octopus`. Nevertheless, since the saturation is very sensitive to the value of p there is still room for improvement in the future.

6 Periodic systems

DFT has been extensively applied to bulk systems, as much as it has been to clusters or molecules. TDDFT for solids, however, has a smaller history [42]. We intend to provide a tool for DFT and TDDFT on extended systems. In the definition of "extended systems," however, we include systems of intermediate dimensionality: systems that are periodic in one and two dimensions. These systems are still 3-dimensional (3D), but their quantum properties are those of a finite system in one or more directions, and those of a periodic system in the remaining directions.

It is possible to implement periodic boundary conditions also in real space, but we have to take special care of (i) the proper implementation of the the operators that are non-local in real space, and (ii) the correct treatment of the long-range Coulomb interaction. Regarding the first issue, we must worry about the differential operators (i.e., gradient and Laplacian), and the non-local components of the pseudopotentials. In both cases, the action of the operator on a function for a given point may need the values of the function at points that belong to a neighboring cell. The periodicity is thus enforced by identifying the "mirror" points.

Regarding the second issue – the correct treatment of the long-range Coulomb interaction – it is convenient to resort to a dual methodology, that allows to move back and forth from real to reciprocal space. In particular, the integration of Poisson's equation is more conveniently performed in Fourier space, but it is easier to impose different boundary conditions in different directions in real space.

6.1 Implementation details for bulk systems

Most of the numerical machinery described in Section 2 for finite systems can be also be used for periodic systems. In the following we will just review the main differences.

Kinetic term. For what concerns the kinetic part of the Hamiltonian, for periodic systems, we have to modify the kinetic operator used for finite systems. The feature that remains common to both cases is that, differently from what happens in plane waves codes, the kinetic energy is entirely calculated in real space. We must however remember that only the periodic part $u_{n\mathbf{k}}(\mathbf{r} + \mathbf{L}) = u_{n\mathbf{k}}(\mathbf{r})$ of the Bloch states $\psi_{n\mathbf{k}}(\mathbf{r}) = \mathrm{e}^{-i\mathbf{k}\cdot\mathbf{r}}u_{n\mathbf{k}}(\mathbf{r})$ is used as the working quantity within the cell, and, accordingly, the kinetic operator used for finite systems has to be modified in the following way:

$$\hat{T} = -\frac{1}{2}\nabla^2 \to \hat{T}_{\mathbf{k}} = -\frac{1}{2}(\nabla^2 + 2i\mathbf{k}\cdot\nabla - k^2). \tag{53}$$

External potential The total local part of the ionic potential of the infinite system is given by

$$v^{\mathrm{local}}(\vec{r}) = \sum_{\vec{n}\in P}\sum_{\alpha}^{N_a} v_{\alpha}^{\mathrm{local}}(|\vec{r} - \vec{d}_{\alpha} - \vec{L}_{\vec{n}}|) . \tag{54}$$

The inner sum runs over the N_a atoms of the unit cell: the index α runs over the atoms in the unit cell, and $\vec{d}_{\alpha}$ indicates the position of the α-th atom. We also use the notation $\vec{L}_{\vec{n}}$ to mean

$(n_x \vec{L}_x, n_y \vec{L}_y, n_z \vec{L}_z)$, and the outer sum is just the sum over the set $\{P\}$ of all the cells allowed by the Born-Von Kármán periodic-boundary conditions.

Evaluation of this expression either in real space or in Fourier space leads to well known convergence problems. The solution consists in splitting $v_\alpha^{\text{local}}(\vec{r})$ into a short range, and a long range part. The long range tail of each atomic potential must behave asymptotically like Z_α/r, where Z_α is the number of valence electrons for the atom α, and the long range part can be chosen in such a way that its Fourier transform is analytical, adopting a suitable representation. This representation is obviously not unique.

A convenient representation turns out to be the following:

$$v_\alpha^{\text{local}}(r) = \Delta v_\alpha(r) - Z_\alpha \frac{\text{erf}(ar)}{r}, \tag{55}$$

where a is chosen in such a way that $\Delta v_\alpha(r)$ is sufficiently localized within the cell, but is also well approximated by its Fourier series when it is truncated to N_i points per each i direction.

The Fourier transform can be performed numerically on the localized part, and analytically on the long range part

$$v_\alpha^{\text{local}}(G) = 4\pi \int_0^R dr \, r^2 \frac{\sin(Gr)}{Gr} \Delta v_\alpha(r) - 4\pi Z_\alpha \frac{\exp\left(-G^2/4a^2\right)}{G^2}. \tag{56}$$

Alternatively, the term $\Delta v_\alpha(r)$ can be directly handled in real space.

Hartree potential   Let us now turn our attention to the Hartree part of the potential. The solution of Poisson's equation in real space can be achieved, for example, with a conjugated gradient minimization method (see discussion in Section 2.2), but, for infinite systems, it is more convenient to transpose the problem to Fourier space, where we can take advantage of the efficient Fast Fourier Transform, that scales like $N \log(N)$ with the number of grid points N. Applying the convolution theorem, we can write Eq. (8) in Fourier space as

$$v_{\text{Hartree}}(\vec{G}) = n(\vec{G})w(G), \tag{57}$$

where $v(G)$ is the Fourier transform of the Coulomb interaction

$$w(G) = \frac{4\pi}{G^2}. \tag{58}$$

The treatment of the singular point $G = 0$ is particularly simple in the case of bulk crystals, since $v(G = 0)$ corresponds to the average value of the potential, which is determined up to an arbitrary constant, and it can set to 0 by observing that the overall charge neutrality of the unit cell imposes $v(G = 0) = 0$. Note that, as the density is periodic, Eq. (57) needs to be evaluated only at the reciprocal primitive vectors $\vec{G}$. The case of systems that are periodic in less than three dimensions is considered below.

6.2   Systems with reduced periodicity: the cutoff problem

In this sub-section we call *nD-periodic* a 3D system, that can be considered infinite and periodic in n dimensions, being finite in the remaining $3 - n$ dimensions. In order to simulate this kind

of systems, a commonly adopted approach is the supercell approximation. In the supercell approximation the physical system is treated as a fully 3D-periodic one, but a new unit cell (the supercell) is built in such a way that some extra empty space separates the periodic replica along the direction(s) in which the system is to be considered as finite.

This approach has several major drawbacks. For instance, it is well known that the response function of an overall neutral solid of molecules is not equal, in general, to the response of the isolated molecule, and converges very slowly to it, when the amount of vacuum in the supercell is progressively increased [42, 60]. Another problem arises when studying slabs, as a layered system (i.e., a supercell) is in fact equivalent to an effective chain of capacitors. These issues become particularly evident in the approaches that involve the calculation of non-local operators or response functions because, in these cases, two supercells may effectively interact even if their charge densities do not overlap at all. Moreover, even in those cases in which good convergence can be achieved, the supercell can be considerably larger than the system, affecting the performance, and wasting computational resources.

Some of the available methods used to avoid these problems have been mentioned in Sec. 2.2, but, with special regard to the periodic case, and considering that the Fourier space method is still the fastest available to solve the Poisson problem, some of us [61] have recently developed a new reciprocal space analytical method to cutoff the long range interactions in supercell calculations, extending previous works for finite systems [14]. This method has been implemented and tested in `octopus`.

Our goal is to transform the 3D-periodic Fourier representation of the Hartree potential

$$v_{\text{Hartree}}(\vec{G}) = n(\vec{G})w(\vec{G}),\tag{59}$$

into the modified one

$$\tilde{v}_{\text{Hartree}}(\vec{G}) = \tilde{n}(\vec{G})\tilde{w}(\vec{G}),\tag{60}$$

such that all the interactions among the undesired periodic replica of the system disappear. The present method is a generalization of the method proposed by Jarvis and collaborators [62] for the case of a finite system.

In order to build this representation, we want to: (i) define a screening region $\mathcal{D}$ around each charge in the system, out of which there is no Coulomb interaction; (ii) calculate the Fourier transform of the desired effective interaction $\tilde{w}(r)$, that equals the Coulomb potential in $\mathcal{D}$, and is 0 outside $\mathcal{D}$

$$\tilde{w}(r) = \begin{cases} \frac{1}{r} & \text{if } r \in \mathcal{D} \\ 0 & \text{if } r \notin \mathcal{D} \end{cases}.\tag{61}$$

Finally, we must (iii) modify the density $n(\vec{r})$ in such a way that the effective density is still 3D-periodic, so that the convolution theorem can be still applied, but densities belonging to undesired images are not close enough to interact through $\tilde{w}(r)$.

The choice of the region $\mathcal{D}$ for step (i) is suggested by symmetry considerations. It is a sphere (or radius R) for finite systems, an infinite cylinder (of radius R) for 1D-periodic systems, and an infinite slab (of thickness $2R$) for 2D-periodic systems.

166

Step (ii) means that we have to calculate the modified Fourier integral

$$\tilde{w}(\vec{G}) = \int \mathrm{d}^3 r \, \tilde{w}(r) e^{-\mathrm{i}\vec{G}\cdot\vec{r}} = \int_{\mathcal{D}} \mathrm{d}^3 r \, w(r) e^{-\mathrm{i}\vec{G}\cdot\vec{r}}. \tag{62}$$

Still, we have to avoid that two neighboring images interact by taking them far away enough from each other. The cutoff functions are analytical in Fourier space except some particular sets of points (the $G_x = 0$ plane in the 1D-periodic case, and the $G_\parallel = 0$ plane in the 2D-periodic case), for which a suitable limiting procedure has to be followed in order to get finite results (explained in Ref. [61]). The results of the integral (62) are the following

- 0D-periodic

$$\tilde{w}^{0D}(G) = \begin{cases} \frac{4\pi}{G^2}[1 - \cos(GR)] & \text{for } G \neq 0 \\ 2\pi R^2 & \text{for } G = 0 \end{cases} \tag{63}$$

- 1D-periodic $(G_\perp = \sqrt{G_y^2 + G_z^2})$

$$\tilde{w}^{1D}(G_x, G_\perp) = \begin{cases} \frac{4\pi}{G^2}\left[1 + G_\perp R J_1(G_\perp R) K_0(|G_x|R) \\ \quad -|G_x| R J_0(G_\perp R) K_1(|G_x|R)\right] & \text{for } G_x \neq 0 \\ -4\pi \int_0^R \mathrm{d}r \, r J_0(G_\perp r) \log(r) & \text{for } G_x = 0 \text{ and } G_\perp > 0 \\ -\pi R^2 (2\log(R) - 1) & \text{for } G_x = 0 \text{ and } G_\perp = 0 \end{cases} \tag{64}$$

- 2D-periodic $(G_\parallel = \sqrt{G_x^2 + G_y^2})$

$$\tilde{w}^{2D}(G_\parallel, G_z) = \begin{cases} \frac{4\pi}{G^2}\left[1 + e^{-G_\parallel R}\left(\frac{|G_z|}{G_\parallel}\sin(|G_z|R) - \cos(|G_z|R)\right)\right] & \text{for } G_\parallel \neq 0 \\ \frac{4\pi}{G_z^2}\left[1 - \cos(|G_z|R) - G_z R \sin(|G_z|R)\right] & \text{for } G_\parallel = 0 \text{ and } G_z \neq 0 \\ -2\pi R^2 & \text{for } G_\parallel = 0 \text{ and } G_z = 0 \end{cases} \tag{65}$$

A suitable supercell consists in increasing the cell in the non-periodic directions (in the 1D-periodic case the supercell size is actually $(1 + \sqrt{2})L$, and in the 0D-periodic it is $(1 + \sqrt{3})L$), and setting to zero the density in this extended area. Again, since the density naturally falls off to zero at the border of a finite system, doubling the cell size in all periodic directions is sufficient.

Figure 6 illustrates the effect of the cutoff on the potentials. The left panel shows the ionic potential, the Hartree potential, and their sum for a Si atom in a parallelepiped supercell with side lengths of 2.5, 11, and 11 a.u. respectively in the x, y and z directions. No cutoff is used here. The ionic potential is roughly behaving like $1/r$ in the area not too close to the nucleus (where the pseudopotential takes over). The total potential, on the other hand, falls off rapidly to an almost constant value at around 4 a.u. from the nuclear position, by effect of the electron screening.

In the right panel of Fig. 6 the cutoff is applied to the all the potentials consistently. The radius of the cylinder is $R = 5.5$ a.u. such that there is zero interaction among the replica of the system along the y and z axes. The ionic potential now behaves like it is expected for a potential of
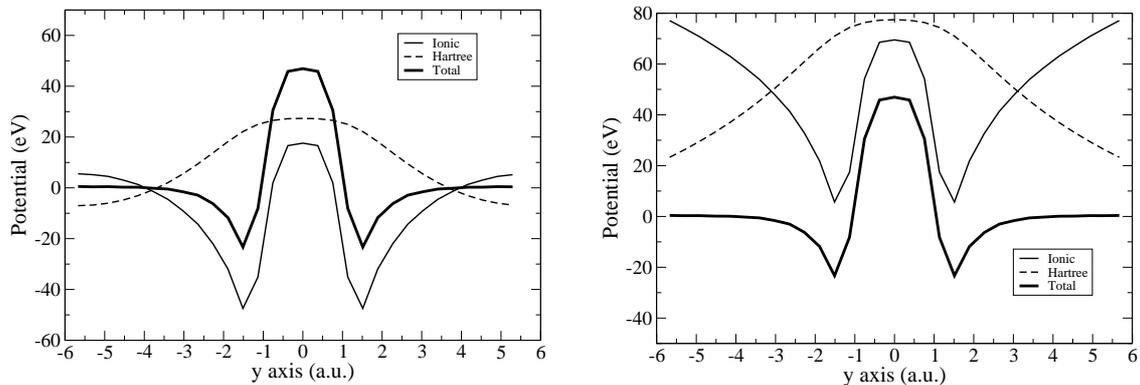
167

Figure 6: Calculated total and ionic and Hartree potentials for a 3D-periodic (left) and 1D-periodic (right) Si chain.
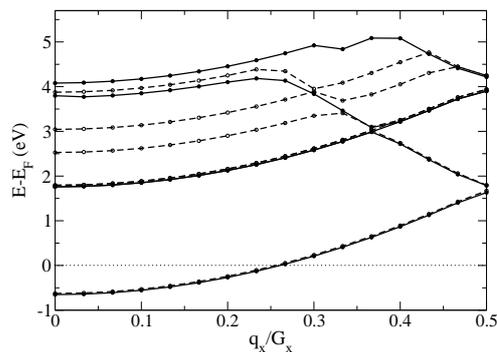

Figure 7: Effect of the cutoff in a Na linear chain in a supercell size of 7.5x19x19 a.u. The bands obtained with an ordinary supercell calculation with no cutoff (dashed line) are compared to the bands obtained applying the 1D cylindrical cutoff (solid line).

a chain, i.e. diverges logarithmically, and is clearly different from the latter case. Nevertheless, the sum of the ionic and Hartree potential is basically the same as for the 3D-periodic system. In the static case the two band structures are found to be the same, confirming that, as far as static calculations are concerned, the supercell approximation is good, provided that the supercell is large enough. In static calculations, then, the use of our cutoff only has the effect of allowing us to eventually use a smaller supercell, which provides clear computational savings. In the case of the Si-chain a full 3D calculation would need a cell size of 38 a.u. whereas the cutoff calculation would give the same result with a cell size of 19 a.u. Of course, when more delocalized states are considered, like higher energy unoccupied states, larger differences are observed with respect to the supercell calculation.

In Fig. 7 a Na chain with lattice constant 7.5 a.u. is considered in a cell of 7.5x19x19 a.u., and the effect of the cutoff on the occupied and unoccupied stated is shown. As expected, the occupied states are not affected by the use of the cutoff, since the density of the system within the cutoff radius is unchanged, and the corresponding band is the same as it is found for an ordinary 3D supercell calculation with the same cell size. However there is a clear effect on the bands corresponding to unoccupied states, and the effect is larger the higher the energy of the states. In fact, the high energy states, and the states in the continuum are more delocalized, and therefore the effect of the boundary conditions is more sensible.

168

In summary, the proposed cutoffs are functions in Fourier space, that are used as a multiplicative factor to screen the bare Coulomb interaction. The functions are analytic everywhere but in a sub-domain of the Fourier space that depends on the periodic dimensionality. In Ref. [61] we show that the divergences that lead to the non-analytical behavior can be exactly canceled when both the ionic and the Hartree potential are properly screened. This technique is exact, fast, and very easy to implement in already existing supercell codes.

7 Conclusions

`octopus` was officially born on the 1st of January 2002. Since then, the code has grown at a steady pace, both in the number of lines of code (that will soon reach the 50.000 lines of Fortran 90), and in the kind of problems it is able to tackle. In this article we gave a brief overview on the code, mentioning some of the algorithms used and their numerical implementation. Some of the most recent developments were discussed in more detail, namely (i) the use of curvilinear coordinates, that can improve dramatically the efficiency of the calculation; (ii) the multiple parallelization approach, that allows the code to scale in some situations to several hundred processors; and (iii) the extension of the code to periodic systems. Nevertheless, `octopus` is still, and will always be, a work in progress. In fact, our TODO list already includes, among others, (i) the extension to all-electron calculations, either using the Projector Augmented Wave technique, or by using specially crafted curvilinear transformations able to describe adequately the core wave-functions; (ii) the possibility of performing fully-relativistic (i.e., Dirac-level) calculations; (iii) the possibility of using hybrid exchange-correlation functionals; etc.

Note, however, that the code is not important *per se*, but due to the physics and chemistry we can learn from it. We believe that `octopus` has already reached a high level of maturity when it comes to the calculation of linear optical properties in nanostructures. In fact, we, and several other groups around the world, routinely use `octopus` to study the optical spectra of large nanocrystallites, bio- chromophores, and even aromatic molecules with astrophysical implications. `octopus` can also be efficiently used to study the interaction of molecules with strong lasers, to calculate (hyper)polarizabilities, etc. However, experimentalists have nowadays at their disposal numerous probes to study physical systems – infrared, visible and ultra-violet light, X-ray radiation, magnetic fields, electron beams, etc. It would be certainly helpful if a tool could describe consistently this whole plethora of spectroscopies. With `octopus` we are still far from this objective, but by adding new features and by making the code more user friendly, we expect to provide a code that is useful to a large scientific community.

Acknowledgements

References

[1] P. Hohenberg and W. Kohn, Phys. Rev. **136**, B864 (1964); W. Kohn and L. J. Sham, Phys. Rev. **140**, A1133 (1965).

[2] C. Fiolhais, F. Nogueira and M. Marques (Eds.), *A Primer in Density Functional Theory*, Lectures Notes in Physics vol. 620, (Springer, Berlin, 2003); R. M. Dreizler and E. K. U. Gross, *Density Functional Theory*, (Springer, Berlin, 1990); R. G. Parr and W. Yang, *Density Functional Theory of Atoms and Molecules*, (Oxford University Press, New York, 1989).

[3] E. Runge and E. K. U. Gross, Phys. Rev. Lett. **52**, 997 (1984).

[4] M. A. L. Marques, F. Nogueira, C. Ullrich, K. Burke, A. Rubio and E. K. U. Gross (Eds.), *TDDFT, Lecture notes* (Springer Verlag, Berlin, to be published in 2006); E. K. U. Gross and W. Kohn, Adv. Quantum Chem. **21**, 255 (1990); E. K. U. Gross, J. F. Dobson and M. Petersilka, in *Topics in Current Chemistry*, edited by R. F. Nalewajski (Springer, Heidelberg, 1996); M. A. L. Marques and E. K. U. Gross, Annu. Rev. Phys. Chem. **55**, 427 (2004); R. van Leeuwen, Int. J. Mod. Phys. B **15**, 1969 (2001).

[5] J. Leszczynski (Ed.), *Computational Chemistry: Reviews of Current Trends*, vol. 9, (World Scientific, 2005); R. J. Bartlett, *Recent Advances in Computational Chemistry, vol 3: Recent Advances in Coupled Cluster Methods*, (World Scientific, 1997).

[6] W. M. C. Foulkes, L. Mitas, R. J. Needs and G. Rajagopal, Rev. Mod. Phys. **73**, 33 (2001); *Quantum Monte Carlo Methods in Physics and Chemistry*, edited by M. P. Nightingale and C. J. Umrigar (Kluwer, 1999).

[7] A forcibly non-exhaustive list (we only reference the web page, where formal references are to be found):

- ABINIT: `http://www.abinit.org/`
- ADF: `http://www.scm.com/`
- DACAPO: `http://www.camp.dtu.dk/`
- EXC!TING: `http://exciting.sourceforge.net/`
- GAMESS: `http://www.msg.ameslab.gov/GAMESS/GAMESS.html/`
- GAUSSIAN: `http://www.gaussian.com/`
- PWSCF: `http://www.pwscf.org/`
- SIESTA: `http://www.uam.es/departamentos/ciencias/fismateriac/siesta/`
- TURBOMOLE: `www.chem-bio.uni-karlsruhe.de/TheoChem/turbomole/intro.en.html/`
- VASP: `http://cms.mpi.univie.ac.at/vasp/`
- WIEN2K: `http://www.wien2k.at/`

[8] M. A. L. Marques, A. Castro, G. F. Bertsch and A. Rubio, Comp. Phys. Comm. **151**, 60 (2003); More information at `http://www.tddft.org/programs/octopus/`.

[9] W. E. Pickett, Comput. Phys. Rep. **9**, 115 (1989).

[10] N. Troullier and J. L. Martins, Phys. Rev. B **43**, 1993 (1991).

[11] C. Hartwigsen, S. Goedecker and J. Hutter, Phys. Rev. B **58**, 3641 (1998).

[12] M. A. L. Marques, X. López, D. Varsano, A. Castro and A. Rubio, Phys. Rev. Lett. **90**, 258101 (2003); X. López, M. A. L. Marques, A. Castro and A. Rubio, J. Amer. Chem. Soc. **127**, 12329 (2005).

[13] A. T. Brunger and M. Karplus, Proteins **4**, 148, 1988; A. Laio, J. VandeVondele and U. Rothlisberger, J. Chem. Phys, **116**, 6941 (2002).

[14] A. Castro, A. Rubio and M. J. Stott, Can. J. Phys. **81**, 1 (2003).

[15] D. M. Ceperley and B. J. Alder, Phys. Rev. Lett. **45**, 566 (1980); J. P. Perdew and A. Zunger, Phys. Rev. B **23**, 5048 (1981).

[16] J. P. Perdew, Phys. Rev. Lett. **55**, 1665 (1985); J. P. Perdew and Y. Wang, Phys. Rev. B **33**, 8800 (1986); ibid. **40**, 3399 (1989) (E); A. D. Becke, J. Chem. Phys. **84**, 4524 (1986); J. P. Perdew, K. Burke and M. Ernzerhof, Phys. Rev. Lett. **77**, 3865 (1996); ibid. **78**, 1396 (1997) (E).

[17] R. P. Sharp and G. K. Horton, Phys. Rev. **90**, 317 (1953); J. D. Talman and W. F. Shadwick, Phys. Rev. A **14**, 36 (1976).

[18] T. Grabo, T. Kreibich, S. Kurth and E. K. U. Gross, in *Strong Correlations in Electronic Structure Calculations: Beyond the Local Density Approximation*, V. I. Anisimov (Ed.), page 203, (Gordon&Breach, Amsterdam, 2000); E. Engel, in *A Primer in Density Functional Theory*, C. Fiolhais, F. Nogueira and M. A. L. Marques (Eds.), Chapter 2, (Springer, Berlin, 2003).

[19] J. B. Krieger, Y. Li and G. J. Iafrate, Phys. Lett. A **146**, 256 (1990).

[20] S. Kümmel and J. P. Perdew, Phys. Rev. Lett **90**, 043004 (2003); S. Kümmel and J. P. Perdew, Phys. Rev. B **68**, 035103 (2003).

[21] G. Vignale and M. Rasolt, Phys. Rev. Lett **59**, 2360 (1987); G. Vignale and M. Rasolt, Phys. Rev. A **37**, 10685 (1988); G. Vignale, M. Rasolt and D. J. W. Geldart, Adv. Quantum Chem. **21**, 235 (1990); M. Rasolt and G. Vignale, Phys. Rev. Lett. **65**, 1498 (1990); K. Capelle and E. K. U. Gross, Phys. Rev. Lett. **78**, 1872 (1997).

[22] Y. Saad, *Numerical methods for large eigenvalue problems*, (Manchester University Press, Manchester, 1992); Z. Bai, J. Demmel, J. Dongarra, A. Ruhe, H. van der Vorst (Eds.), *Templates for the solution of algebraic eigenvalue problems: A practical guide*, (SIAM, Philadelphia, 2000).

[23] M. P. Teter, M. C. Payne and D. C. Allan, Phys. Rev. B **40**, 12255 (1989); M. C. Payne, M. P. Teter, D. C. Allan, T. A. Arias and J. D. Joannopoulos, Rev. Mod. Phys. **64**, 1045 (1992).

[24] J. Cullum and W. E. Donath, in *Proceedings of the 1974 IEEE Conference on Decision and Control*, pp. 505-509, (New York, 1974); J. Cullum and R. A. Wilboughby, *Lanczos algorithms for large symmetric eigenvalue computations*, vol. 1, (Boston, MA., 1985); J. Cullum and R. A. Willoughby, J. Comp. P. **434**, 329 (1981).

[25] G. L. G. Sleijpen and H. A. van der Vorst, SIAM Review **42**, 267 (2000).

[26] P. H. Dederichs and R. Zeller, Phys. Reb. B **28**, 5462 (1983).

[27] D. D. Johnson, Phys. Rev. B **38**, 12807 (1988); See also C. G. Broyden, Math. Comput. **19**, 577 (1965); D. G. Anderson, J. Assoc. Comput. Mach. **12**, 547 (1964); P. Pulay, Chem. Phys. Lett. **73**, 393 (1980); P. Pulay, J. Comp. Chem. **3**, 556 (1982).

[28] D. R. Bowler and M. J. Gillan, Chem. Phys. Lett. **325**, 473 (2000).

[29] U. von Barth and L. Hedin, J. Phys. C **5**, 1629 (1972).

[30] A. Brandt, *Math. Comp.* **31** 333-390 (1977).

[31] W. L. Briggs, (SIAM, Philadelphia, 1987); P. Wesseling, (Wiley, New York, 1992); T. L. Beck, Rev. Mod. Phys. **72**, 1041 (2000).

[32] M. Heiskanen, T. Torsti T., M. J. Puska, R. M. Nieminen, Phys. Rev. B **63**, 245106 (2001).

[33] Xavier Andrade, *Cálculo de la estructura electrónica por un método multinivel*, Master Thesis, Universidad de Chile, 2004.

[34] C. A. Ullrich, U. J. Gossmann and E. K. U. Gross, Phys. Rev. Lett. **74**, 872 (1995).

[35] A. Castro, M. A. L. Marques and A. Rubio, J. Chem. Phys. **121**, 3425 (2004).

[36] K. Yabana and G. F. Bertsch, Phys. Rev. B **54**, 4484 (1996); For calculation with octopus, see Ref. [12]; also A. Castro, M. A. L. Marques, J. A. Alonso, G. F. Bertsch, K. Yabana and A. Rubio, J. Chem. Phys. **116**, 1930 (2002).

[37] A. Castro, M. A. L. Marques, M. Oliveira and A. Rubio, to be published.

[38] M. E. Casida, in *Recent Advances in Density Functional Methods, Part I*, D. P. Chong (Ed.), page 155, (World Scientific Press, Singapore, 1995); C. Jamorski, M. E. Casida and D. R. Salahub, J. Chem. Phys. **104**, 5134 (1996); M. Petersilka, U. J. Gossmann and E. K. U. Gross, in *Electronic Density Functional Theory: Recent Progress and New Directions*, J. F. Dobson, G. Vignale and M. P. Das (Eds.), (Plenum, New York, 1996); T. Grabo, M. Petersilka and E. K. U. Gross, J. Mol. Structure (THEOCHEM) **501**, 353 (2000).

[39] M. Petersilka, U. J. Gossmann and E. K. U. Gross, Phys. Rev. Lett. **76**, 1212 (1996);

[40] J. F. Dobson, M. J. Bünner and E. K. U. Gross, Phys. Rev. Lett. **79**, 1905 (1997).

[41] M. Petersilka and E. K. U. Gross, Laser Phys. **9**, 105 (1999).

[42] G. Onida, L. Reining and A. Rubio, Rev. Mod. Phys. **74**, 601 (2002).

[43] C. A. Ullrich, S. Erhard and E. K. U. Gross, in *Super Intense Laser Atom Physics (SILAP IV)*, H. G. Muller and M. V. Fedorov (Eds.), pp. 267-284, (Kluwer, Amsterdam, 1996); A. Castro, M. A. L. Marques, J. A. Alonso, G. F. Bertsch and A. Rubio, Eur. Phys. J. D **28**, 211 (2004).

[44] S. Baroni, P. Giannozzi and A. Testa, Phys. Rev. Lett. **58**, 1861 (1987).

[45] S. Baroni, S. de Gironcoli, A. Dal Corso,P. Giannozzi, Rev. Mod. Phys. **73**, 515-562 (2001)

[46] X. Gonze, Phys. Rev. A **52**, 1086 (1995); X. Gonze, Phys. Rev. A **52**, 1096 (1995)

[47] R. M. Sternheimer, Phys. Rev. **96**, 951 (1954); R. M. Sternheimer, ibid. **84**, 244 (1951); R. M. Sternheimer and H. M. Foley, ibid. **92**, 1460 (1953).

[48] X. Gonze, J.-P. Vigneron, Phys. Rev. B **39**, 13120-13128 (1989)

[49] A. Dal Corso, F. Mauri and A. Rubio, Phys. Rev. B **53**, 15638-15642 (1996).

[50] F. Gygi, Phys. Rev. B **48**, 11692 (1993); F. Gygi, Phys. Rev. B **51**, 11190 (1995); F. Gygi and G. Galli, Phys. Rev. B **52**, R2229 (1995).

[51] D. R. Hamann, Phys. Rev. B **51**, 9508 (1995); **54**, 1568 (1996); **56**, 14979 (1997); **63**, 075107 (2001).

[52] J. M. Pérez-Jordá, Phys. Rev. A **52**, 2778 (1995); Phys. Rev. B **58**, 1230 (1998);

[53] E. L. Briggs, D. J. Sullivan, and J. Bernholc, Phys. Rev. B **54** 14362 (1996).

[54] E. Fattal, R. Baer and R. Kosloff, Phys. Rev. B **53**, 1217 (1996).

[55] U. V. Waghmare, H. Kim, I. J. Park, N. Modine, P. Maragakis and E. Kaxiras, Comp. Phys. Comm. **137**, 341 (2001); N. A. Modine, G. Zumbach and E. Kaxiras, Phys. Rev. B **55**, 10289 (1997).

[56] Message Passing Interface Forum, Int. J. of Supercomputing Applications **8**, 165 (1994); M. Snir, S. W. Otto, S. Huss-Lederman, D. W. Walker and J. Dongarra, *MPI: The Complete Reference*, (MIT Press, Cambridge MA, 1995); W. Gropp, E. Lusk, N. Doss and A. Skjellum, Parallel Computing **22**, 789 (1996).

[57] http://www.top500.org

[58] G. Karypis and V. Kumar, SIAM J. on Scientific Computing **20**, 359 (1998); The library is available at http://www-users.cs.umn.edu/~karypis/metis/.

[59] G. Amdahl, AFIPS Conference Proceedings (30), pp. 483-485 (1967).

[60] Sottile, F. Bruneval, A. G. Marinopoulos, L. Dash, S. Botti, V. Olevano, N. Vast, A. Rubio and L. Reining, Int. J. Quantum Chem. **112**, 684 (2005).

[61] C. A. Rozzi, D. Varsano, A. Marini, E. K. U. Gross and A. Rubio, to be published (web preprint at arXiv:cond-mat/0601031).

[62] M. R. Jarvis, I. D. White, R. W. Godby, M. C. Payne, Phys. Rev. **B 56**, 14972 (1997)